Observation of Airplane Flowfields by Natural Condensation Effects

James F. Campbell, Joseph R. Chambers, and Christopher L. Rumsey
NASA Langley Research Center, Hampton, Virginia

Nomenclature

c	= chord, ft
M	= Mach number
p	= static pressure, atm
p_a	= partial pressure of dry air, atm
p_s	= pressure of saturated water vapor, atm
p_v	= partial pressure of water vapor, atm
R	= gas constant
Re	= Reynolds number based on chord
RH	= relative humidity
T	= static temperature, K
x/c	= nondimensional chordwise distance for airfoil
y_v	= mole fraction for water vapor
α	= angle of attack, deg
ρ	= density

Subscripts

ℓ	= local conditions
∞	= freestream conditions

Introduction

TRADITIONALLY, aircraft off-surface flowfields have been observed and diagnosed in wind tunnels with special instrumentation and flow visualization equipment.[1-14] With the advent of highly maneuverable military fighters, the relative importance of these off-surface flows, especially vortical flows, has greatly increased.[15] Thus, the designer now requires more extensive information regarding flow properties and diagnostics. Some progress is being made to visualize and measure such flows in flight.[16-20] However, this area still represents a formidable challenge, which currently limits the scope of wind-tunnel/flight correlation efforts.

When humid air expands around an airplane, it can condense, become visible, and illustrate certain flow patterns, such as the wing-body strake vortices on the F-16 (Fig. 1a). Condensation patterns, which are often seen on transport and fighter airplanes in flight, usually occur without warning because they are very sensitive to atmospheric weather conditions and to aircraft flight conditions. Photographs of condensed flow patterns have traditionally been obtained by pilots or professional photographers who generally have not been aware of their potential research value.

To date, naturally occurring condensation has not been critically examined as a technique for flight flow visualization, as evidenced by the absence of studies in flow visualization conferences[21-24] and flight testing conferences.[25-27] Hence, there is a need to determine what condensation patterns can be seen in flight, and to provide interpretation and analysis of what the patterns mean in order to assess the potential for developing the condensation phenomenon into an operational flight flow visualization technique. To help meet this need, NASA Langley Research Center recently conducted an extensive solicitation of visual material showing condensation effects on aircraft from professional aircraft photographers, military squadrons, industry peers, and aviation enthusiasts. Over 300 photographs and several video tapes were obtained from domestic sources as well as European, Canadian, Japanese, and Australian sources. This collection of photographs will be published in a NASA special publication, which will be useful to a broad audience.

The objective of the present paper is to provide samples of the flight photographs, to illustrate the types of flow patterns that have been visualized, and to present qualitative correlations with computational and wind-tunnel results. Initially, the condensation process will be discussed, including a review of relative humidity and vapor pressure and factors that determine the presence of visible condensate. Next, output from computer code calculations will be post-processed using water-vapor relationships to determine if computed values of relative humidity in the local flowfield correlate with the qualitative features of the in-flight condensation patterns. Finally, a series of flight flow patterns will be presented to illustrate the

James F. Campbell is a Senior Aerospace Engineer in the Transonic Aerodynamics Branch. He is an expert in the aerodynamics of separation-induced vortex flows and was responsible for the Vortex Flow Aerodynamics Conference at NASA Langley Research Center in 1985. He has been employed at Langley Research Center since 1963. Dr. Campbell received his B.S. degree in Aerospace Engineering from Mississippi State University, and his Ph.D. degree from Virginia Polytechnic Institute in 1971. He served as the founding chairman of the Applied Aerodynamics Technical Committee, and is currently a member of the AGARD Fluid Dynamics Panel and an Associate Fellow of AIAA.

Joseph R. Chambers is the Assistant Chief of the Flight Applications Division, which conducts fundamental and applied research on the aerodynamics and flight dynamics of advanced military and civil aircraft. He is an internationally recognized authority in the field of high-angle-of-attack flight dynamics, and he received the AIAA Mechanics and Control of Flight Award in 1975 for his research accomplishments in this area relative to military aircraft. He has been employed at NASA Langley Research Center since 1962. Mr. Chambers received his B.S. degree from Georgia Tech and his M.S. degree from the Virginia Polytechnic Institute.

Christopher L. Rumsey is a Research Scientist in the Analytical Methods Branch. He has helped to develop a Navier-Stokes code with particular application to high-angle-of-attack and separated-flow aerodynamic problems. He has been employed at NASA Langley Research Center since 1983. Mr. Rumsey received his B.S. and M.E. degrees in Aerospace Engineering from Rensselaer Polytechnic Institute, and is a Member of AIAA.

Presented as Paper 88-0191 at the AIAA 26th Aerospace Sciences Meeting, Reno, NV, Jan. 11-14, 1988; received Feb. 19, 1988; revision received Sept. 20, 1988.

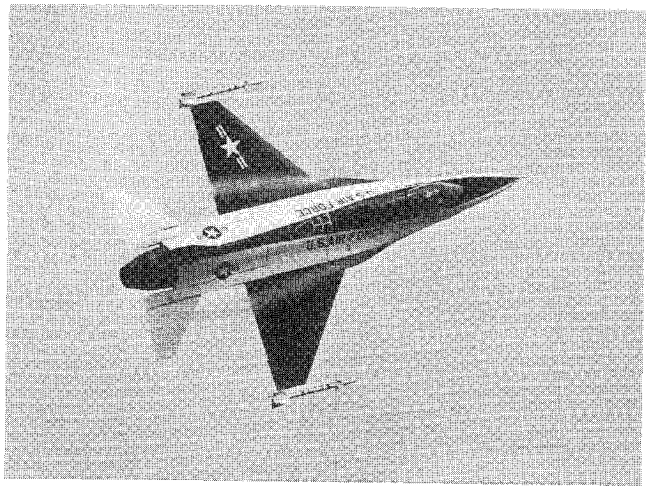

a) In-flight condensation pattern of F-16 wing-body strake vortices (1975)

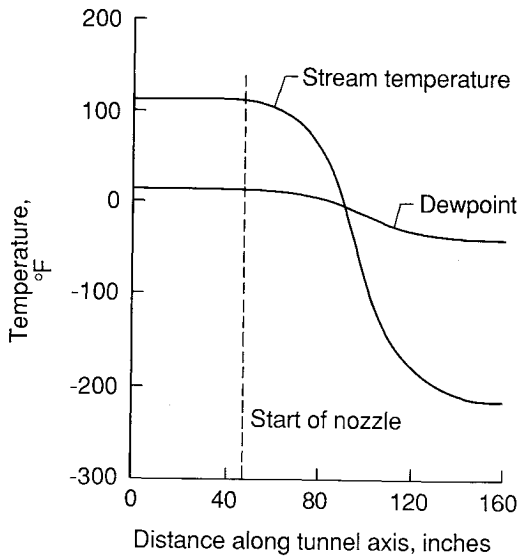

b) Expansion of moist air in a supersonic wind tunnel

Fig. 1 In-flight condensation has not been utilized as a research technique to visualize airplane flowfields.

variety of flowfields that can be visualized, and several will be compared with tunnel results.

Principles of Relative Humidity

Research studies of moist and condensing flows have been conducted for many years to understand the effects of condensation in high-speed wind tunnel flows[28-31] and on wind tunnel models.[32-36] These studies have provided valuable information about condensation effects on tunnel calibration, data accuracy, and tunnel operational envelope, where condensation first occurs on a model.

An example of the expansion of moist air in a supersonic tunnel, Fig. 1b, is from Pope and Goin.[29] The figure shows the variation of stream temperature and dewpoint along the axis, where the flow is expanding to $M_\infty = 2.56$ from a total temperature of 110°F and a total pressure of 25 psia, and with the dewpoint $= -1$°F at 1 atm. Condensation is possible in the expanding tunnel flow once the stream temperature drops below the dewpoint temperature.

Detailed modeling of the exact condensation process is beyond the scope of the current paper. However, relative humidity is used as a qualitative indicator of where the flow is likely to begin to condense ($RH \geq 1$) or where already existing condensate is likely to begin to evaporate ($RH \leq 1$). An existing theoretical method was used to compute flowfields, which were post-processed to determine relative humidity in the local flow. Thus, it was possible to examine the sensitivity of relative humidity to changes in flow pressure and temperature during expansions and compressions.

Derivation of Equations

The objective of the following derivation is to obtain an expression for local relative humidity as a function of freestream relative humidity and local and freestream values of static pressures and temperatures. In this way, relative humidity will be given as a function of local variables, which are computed by the Euler or Navier-Stokes codes.

The equations used in this analysis can be derived by taking moist air as a mixture of two gases, dry air and water vapor. For moist air, Wegener and Mack[28] found that the ratio of specific heat was a constant and was approximately 1.4 for the range of pressures and temperatures of this study. In addition, Van Wylen[37] determined that the perfect gas law can be used for the mixture as well as for the individual components of the mixture.

$$p = \rho RT \tag{1}$$

Since each component of the gas mixture has a partial pressure, the static pressure in the flow is given by the sum of p_a and p_v:

$$p = p_a + p_v \tag{2}$$

The expressions for local and freestream static pressures are:

$$p_\ell = p_{a,\ell} + p_{v,\ell} \quad \text{and} \quad p_\infty = p_{a,\infty} + p_{v,\infty} \tag{3}$$

Following Eq. (2.1) from Wegener and Mack,[28] relative humidity is defined as

$$\Phi = 100\ RH \tag{4}$$

where RH is the ratio of p_v to p_s at the local temperature of the air.

$$RH = p_v/p_s \tag{5}$$

Dewpoint is the temperature at which water vapor may begin to condense, and occurs when RH reaches a value of 1. For aircraft in flight, any small particulates in the air, such as dust, pollution, etc., will provide the seed particles for condensation to commence. This is the heterogeneous process described by Wegener and Mack[28] and Hall.[34] When the temperature has dropped below the dewpoint, the air is considered supercooled.

First, define relative humidity for freestream and local flow conditions:

$$RH_\infty = \left(\frac{p_v}{p_s}\right)_\infty = \frac{p_{v,\infty}}{p_{s,\infty}} \quad \text{at} \quad T_\infty \tag{6}$$

$$RH_\ell = \left(\frac{p_v}{p_s}\right)_\ell = \frac{p_{v,\ell}}{p_{s,\ell}} \quad \text{at} \quad T_\ell \tag{7}$$

Following Van Wylen,[37] define y_v as the ratio of p_v to the sum of the partial pressures, which is p.

$$y_v = p_v/p \quad \text{or} \quad p_v = y_v p \tag{8}$$

The mole fraction is a constant until condensation starts. A more detailed discussion is given by Wegener and Mack[28] who used a mixing ratio.

At freestream and local conditions,

$$p_{v,\infty} = y_{v,\infty} p_\infty \tag{9}$$

$$p_{v,\ell} = y_{v,\ell} p_\ell \tag{10}$$

where p_∞ and p_ℓ are freestream and local static pressures, respectively. Substitute for partial pressure of water vapor in the freestream, Eq. (9), into Eq. (6) to get:

$$RH_\infty = \frac{p_{v,\infty}}{p_{s,\infty}} = \frac{y_{v,\infty} p_\infty}{p_{s,\infty}} \tag{11}$$

Solving for freestream mole fraction,

$$y_{v,\infty} = RH_\infty \frac{p_{s,\infty}}{p_\infty} \tag{12}$$

Similarly, for local flow,

$$RH_\ell = \frac{p_{v,\ell}}{p_{s,\ell}} = \frac{y_{v,\ell} p_\ell}{p_{s,\ell}} \tag{13}$$

Taking the mole fraction to be constant throughout the flow, $y_{v,\ell} = y_{v,\infty}$, and substitute for $y_{v,\ell}$ in Eq. (13). Then

$$RH_\ell = \frac{y_{v,\infty} p_\ell}{p_{s,\ell}} \tag{14}$$

Hence,

$$y_{v,\ell} = y_{v,\infty} = RH_\infty \frac{p_{s,\infty}}{p_\infty} \tag{15}$$

Substitute Eq. (15) into Eq. (14) to get

$$RH_\ell = RH_\infty \frac{p_\ell}{p_\infty} \frac{p_{s,\infty}}{p_{s,\ell}} \tag{16}$$

The vapor-pressure curve for water is presented in Fig. 2, which defines the conditions of static pressure and temperature under which a vapor and liquid can coexist; that is, where $RH = 1$. For $RH > 1$, condensation can begin and for $RH < 1$, evaporation can take place. The constants used in the expression,

$$\log_{10} p_s(\text{atm}) = 6.064 - \frac{2263}{T(\text{K})} \tag{17}$$

were obtained from Wegener.[30] This equation defines a single function to use with freestream and local values of temperature to obtain values for $p_{s,\infty}$ and $p_{s,\ell}$. Substituting Eq. (17) into Eq. (16) yields

$$RH_\ell = RH_\infty \frac{p_\ell}{p_\infty} 10^{\left[-\frac{2263}{T_\infty}\left(\frac{T_\ell/T_\infty - 1}{T_\ell/T_\infty}\right)\right]} \tag{18}$$

Thus, RH_ℓ is a linear function of RH_∞, freestream and local pressure, and a log function of local and freestream temperatures. Therefore, increasing p_ℓ and decreasing T_ℓ increases RH_ℓ, while decreasing p_ℓ and increasing T_ℓ decreases RH_ℓ.

Two-Dimensional Navier-Stokes Example

An example of a calculated result for RH_ℓ is presented in Fig. 3 for the upper surface flow of an airfoil at transonic conditions. The two-dimensional Navier-Stokes code of Rumsey et al.[38] was used to solve the flowfield about an RAE 2822 airfoil at $\alpha = 2.81$ deg, $M_\infty = 0.75$, $T_\infty = 280$ K, $Re = 6.2 \times 10^6$, and $RH_\infty = 0.85$. The output from the code was post-processed to obtain the values for relative humidity,

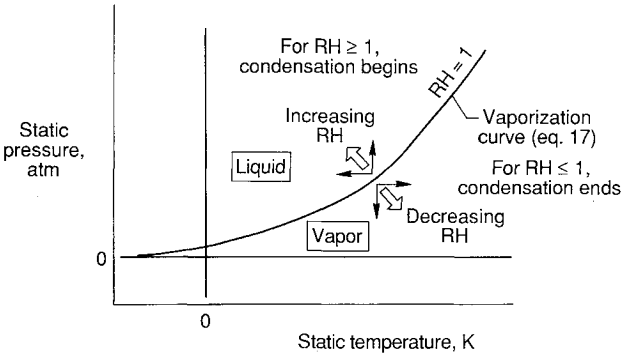

Fig. 2 Pressure of saturated water vapor as a function of temperature.

and, as a result, there is no effect of condensation actually taking place in this calculation. Condensing flow does affect the local flow properties, but accounting for this in a full calculation is beyond the scope of the paper. Contour plots of Mach number and relative humidity are shown in Figs. 3a and 3b, respectively. The relative humidity contour is very similar to the Mach contour because relative humidity is a function of Mach number.[28] The flow expands from the subsonic freestream to supersonic Mach numbers over the airfoil, with a maximum value of about 1.30 near the airfoil surface in front of the shock wave. The flow then compresses through the shock to subsonic flow at the trailing edge. Correspondingly, the relative humidity increases rapidly in the expansion portion of the airfoil flow, reaching a value of about 20 in front of the shock, then decreases rapidly through the shock to a value less than 1.0 at the trailing edge.

Although it is difficult to see in the contour plot, the calculations showed that the boundary-layer flow adjacent to the airfoil surface had higher temperatures, which resulted in low values of RH_ℓ. This result is consistent with the analysis of Wegener and Mack,[28] who observed that a shear flow is one of the ways to evaporate condensed flow back into a vapor.

The flow Mach number, static pressure and temperature, and relative humidity are presented along a streamline through the flow in Figs. 3c and 3d. The properties along the streamline show that the flow expands quickly from the nose region, resulting in rapid increases in M_ℓ, decreases in local pressure and temperature, and increases in RH_ℓ. These trends continue until maximum or minimum values are reached for all of the properties just in front of the shock wave. Rapid flow compressions through the shock wave result in large increases in static pressure and temperature, and a correspondingly significant decrease in the relative humidity.

Recalling Eq. (18), decreasing temperature results in higher values of RH_ℓ through a logarithmic function while decreasing pressure results in lower values of RH_ℓ through a linear function. Therefore, a given change in temperature has a much greater effect on the value of RH_ℓ than a proportional change in pressure. Figures 3c and 3d demonstrate this trend. The temperature decrease along the streamline in front of the shock results in a strong rise in RH_ℓ in spite of the pressure decrease. Through the shock, the sharp temperature rise results in the drop of RH_ℓ, in spite of rising pressures. This is the same trend for the relative importance of temperature over pressure that Pope and Goin[29] described for a supersonic nozzle expansion presented in Fig. 1b.

The extremely high local values of relative humidity are not realistic since the flow can begin condensing at $RH_\ell = 1$, and will condense even without seed particles when RH_ℓ is about 4, when homogeneous nucleation occurs.[30] Once condensation occurs, the resulting heat released keeps the value of RH_ℓ roughly between 1 and 4. While the $RH_\ell > 4$ is unrealistic, the relative magnitudes of RH_ℓ indicate where condensation should occur first in the flow and be the most prominent.

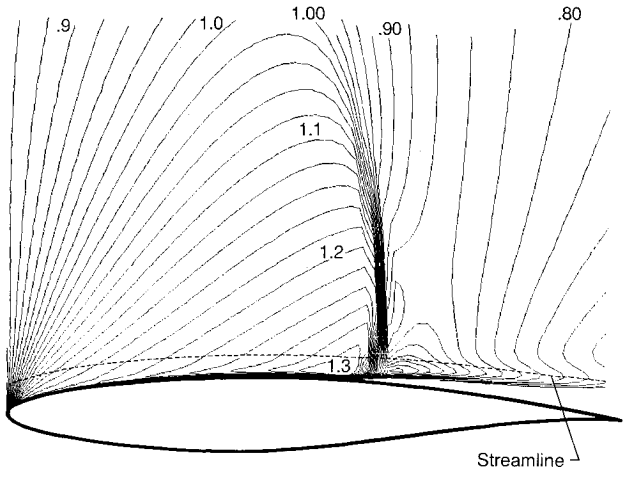

a) Mach number contours

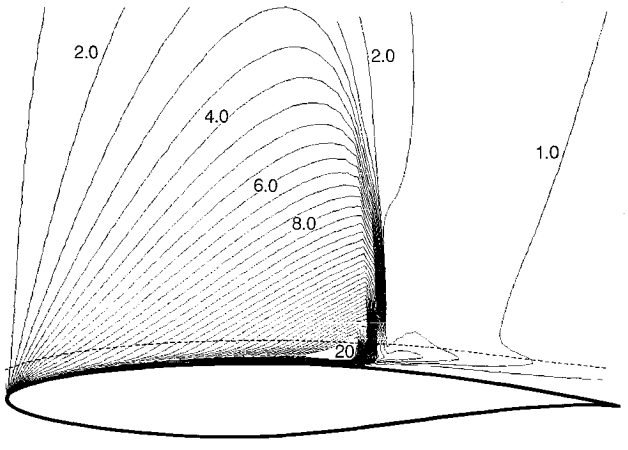

b) Relative humidity contours

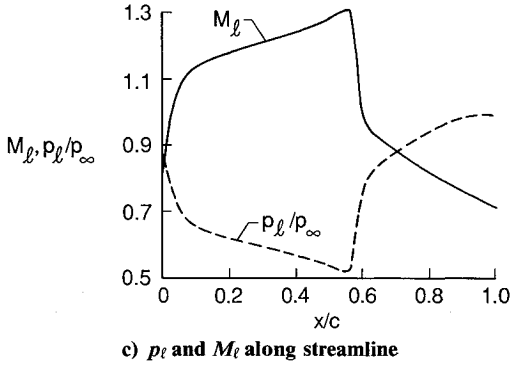

c) p_ℓ and M_ℓ along streamline

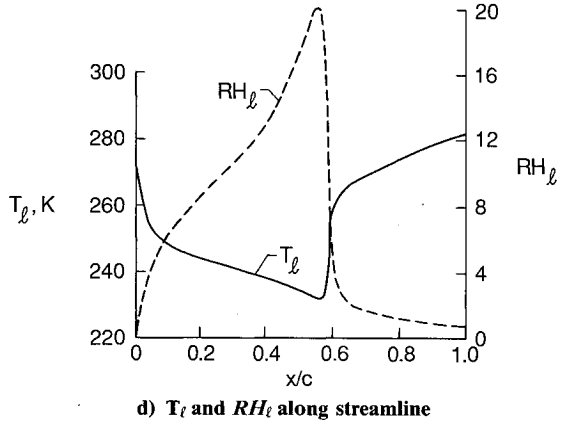

d) T_ℓ and RH_ℓ along streamline

Fig. 3 Two-dimensional Navier-Stokes solution and corresponding flow properties along a streamline for an RAE 2822 airfoil; $M_\infty = 075$, $T = 280$ K, $RH_\infty = 085$, $\alpha = 2.81$ deg, $Re = 6.2 \times 10^6$.

In order to attain visual patterns of calculated relative humidity for different types of airplane flows, additional computational results are presented in the next section.

Correlation of Flight Condensation Patterns

Three flight condensation patterns were found to be common for a variety of airplanes: the spanwise "gull" pattern for swept wing-bodies, expansion and shock patterns for configurations with transonic flow, and leading-edge separation-induced vortex flow for slender wings. Calculations of relative humidity were obtained for examples of each of these three types of flowfields to compare qualitatively with the condensation patterns in flight. These relative humidity calculations were made by post-processing existing solutions that were calculated with a standard computer code that does not take into account the possibility of condensation. The existing solutions were not calculated using the specific geometry of the flight examples, but are believed to be generally representative of the classes of flow. The computer code used to generate results for the three types of flowfields was an upwind-biased, finite-volume scheme (see Rumsey et al.,[38] Anderson et al.,[40] Thomas and Anderson,[41] and Thomas et al.[43]). The code could be run using generalized coordinates in either two or three dimensions with either the Euler or the Navier-Stokes equations. Values of $RH_\infty = 0.85$ and $T_\infty = 280$ K used for these calculations were arbitrarily chosen to represent a typical atmospheric condition.

All color graphics are shown with a light blue background. Values for RH_ℓ ranged from black for the minimum values shown to white for the maximum values shown. Geometries are shown as gray for the wing-body and delta-wing configurations, and as brown for the airfoil.

Gull Patterns

A flow pattern observed on a number of swept wing airplanes during maneuvering flight is the spanwise "gull" shape shown in Fig. 4a. The photograph is of the transonic aircraft technology (TACT) airplane at $M_\infty = 0.82$ during a 3.3 g turn with $\alpha = 6.9$ deg. The flow is not condensed over the fuselage, but builds up progressively from the wing root to a maximum about mid-span, then diminishes as the wing tip is approached. There is no apparent condensation on the lower wing surface, and the wing tip vortices stream rearward from the tips. The fact that the trailing-edge region of the wing is visible indicates that flow evaporation has taken place in that area. For this flight condition, flight data[39] indicate that there is a shock wave over the wing, which, as noted in Fig. 3, would increase temperature, decrease relative humidity, and induce evaporation.

The calculated relative humidity pattern (Fig. 4b) was obtained by post-processing three-dimensional Euler code results of Anderson et al.[40] and Thomas and Anderson[41] for a swept wing-body configuration (Boeing 747-200) at $M_\infty = 0.84$, $T_\infty = 280$ K, $\alpha = 2.4$ deg, and $RH_\infty = 0.85$. The pattern was generated for spanwise planes of RH_ℓ, ranging in value from 1.6–12.0. For clarity, values of $RH_\ell < 1.6$ are not shown. The calculation results in a spanwise pattern on the wing and body similar to that observed for the flight condensation on the TACT.

Maximum velocities, and hence minimum temperatures and pressures, occur over the mid-span section of the wing and result in the largest values of RH_ℓ (shown as white). Similar to the results for the RAE 2822 airfoil described in Fig. 3, the temperature change has a greater effect on RH_ℓ than the pressure change. The values of RH_ℓ decrease at the wing root, tip, and trailing-edge due to temperature recovery and in spite of pressure increase. As before, the temperature effect dominates RH_ℓ because it is the stronger function.

Expansion and Shock Patterns

Some of the most dramatic condensation patterns occur at transonic conditions, where the supercritical flow around an

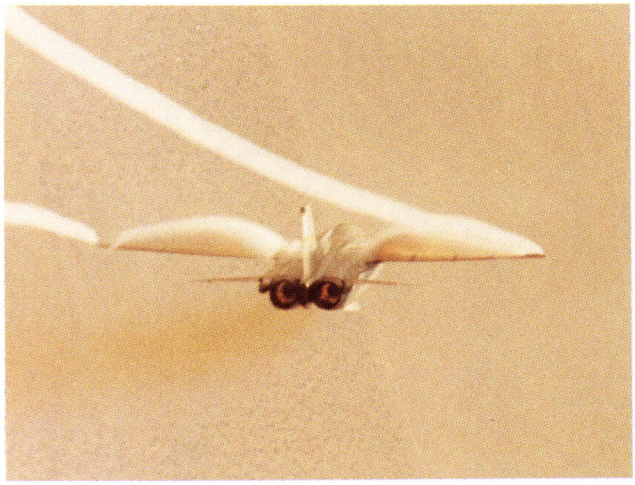

a) Flight condensation

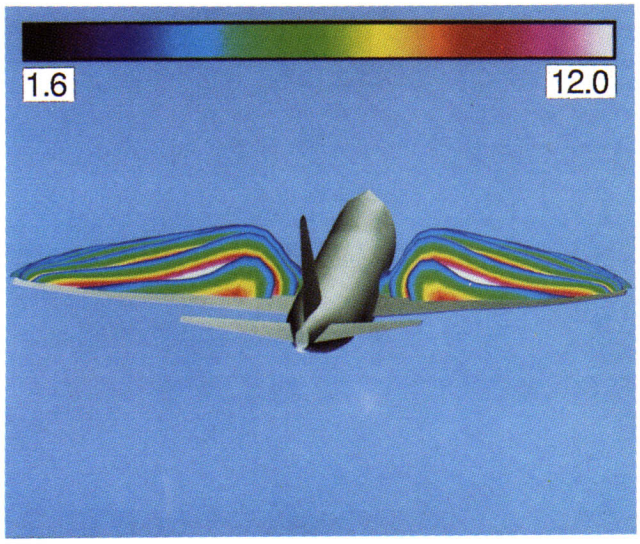

b) Calculated relative humidity

Fig. 4 Comparison of "gull" patterns obtained form flight condensation with those from calculated relative humidity for swept wing-bodies with transonic flow; $M_\infty \approx 0.8$

airplane extends to large vertical distances from the airplane. A good example of this phenomenon is shown in Fig. 5a for an F-14 airplane[42] during level flight at $M_\infty = 0.9$. The freestream flow accelerates to supersonic speeds above and below the wing, causing the flow to condense in the expansion waves in the front portion of the condensation pattern. The aft end of the pattern is created by a shock wave through which the flow is decelerated back to subsonic speeds. Recalling the discussion for Fig. 3, the rapid temperature rise through the shock causes the condensed flow to evaporate. Note also the condensation at the canopy, which indicates an expanded flow in that area.

The two-dimensional Navier-Stokes code results of Rumsey et al.[38] were used to calculate the relative humidity pattern for transonic flow over an NACA 0012 airfoil at $\alpha = 2$ deg with $M_\infty = 0.9$, $T_\infty = 280$ K, $RH_\infty = 0.85$, and $Re = 9 \times 10^6$. RH_ℓ values are shown from 2.0–44.0; RH_ℓ values less than 2.0 are shown as light blue. The calculated pattern is qualitatively similar to the condensed pattern on the F-14 in that it shows expansion regions of supercritical flow and shock waves. Of course, the intent here is not to compare the two-dimensional airfoil solution directly with patterns created by the three-dimensional F-14 geometry, but just to generally illustrate the effects of relative humidity in supercritical flows. Calculating the F-14 flowfield with a three-dimensional transonic code

a) Flight condensation

b) Calculated relative humidity

Fig. 5 Comparison of expansion and shock patterns obtained from flight condensation with those from calculated relative humidity for highly-swept and unswept configurations with transonic flow; $M_\infty = 0.9$.

would provide more specific comparisons between the calculated humidity pattern and inflight condensation. The light blue at the airfoil surface is indicative of the low RH_ℓ values in the boundary layer, which was discussed previously for Fig. 3b.

Leading-Edge Vortex Flow Patterns

In Fig. 6a, leading-edge vortex flows are illustrated by condensed patterns on top of the wings of the Concorde during landing. A comparable pattern of calculated relative humidity (Fig. 6b) was obtained for a 76 deg slender delta wing using the three-dimensional Navier-Stokes code results of Thomas et al.[43] The calculations were made for $M_\infty = 0.3$, $\alpha = 20.5$ deg, $T_\infty = 280$ K, $RH_\infty = 0.85$, and $Re = 0.95 \times 10^6$, and are plotted for RH_ℓ values from 1.0–1.25. Values less than 1.0 are not shown for clarity. The maximum value for RH_ℓ is lower than the previous calculations because of the lower freestream Mach number.

a) Flight condensation

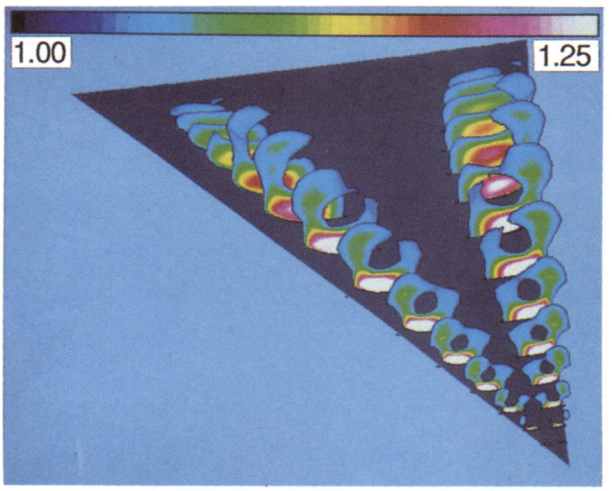

b) Calculated relative humidity

Fig. 6 Comparison of leading-edge vortex patterns obtained from flight condensation with those from calculated relative humidity for slender configurations, low speed.

The calculated relative humidity pattern shows the leading-edge separation-induced vortex system over the delta wing. Flow expansion occurs around the vortex core with the highest RH_ℓ values (white) being under the core. The size of the pattern grows from the apex rearward to about 50% aft, where it reaches a maximum and then diminishes as the trailing edge is reached. This reduction is due to the trailing-edge recovery, with its corresponding rise in temperature and pressure, and is not due to a vortex breakdown. For this configuration, vortex burst occurs at the wing trailing edge at $\alpha \approx 33$ deg according to both the theory of Thomas et al.[43] and the experiments of Hummel.[44] The Concorde's condensation pattern appears to exhibit a similar trailing-edge recovery effect to that calculated for the delta wing as evidenced by the evaporation of condensed vortex flow near the wing trailing edge.

An interesting outcome of the calculated RH_ℓ pattern is that the core region of the vortex appears as a "hole," where RH_ℓ values were less than 1.0 and thus were not plotted. Examination of the flowfield results[43] showed that the core experiences a temperature increase and pressure decrease, compared to just outside the core, which results in a core value for RH_ℓ less than 1.0. This may be an additional explanation of why vortex cores sometimes appear to be hollow or clear, as noted in Figs. 12a and 13a, in addition to the classical explanation of centrifugal effects on core fluid particles.

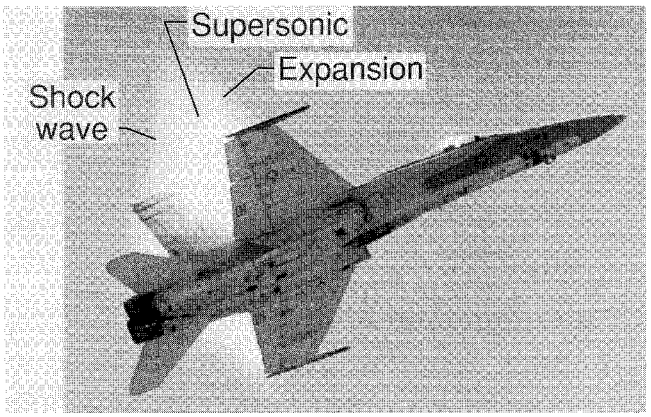

a) F-18, high speed pull up

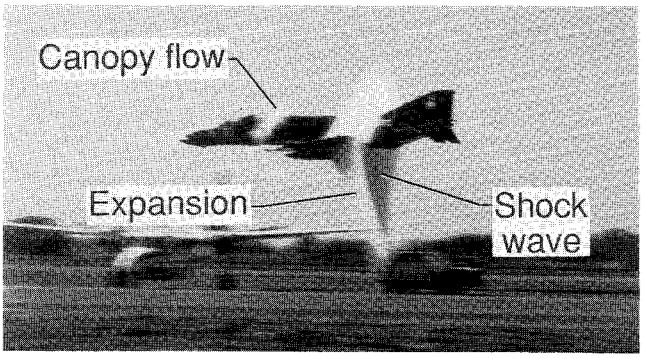

b) F-4, high speed pass on the deck

Fig. 7 Example of transonic flow patterns for several fighter aircraft.

These computations for three different classes of airplane flow suggest that calculations of relative humidity with flowfield codes is a useful way to obtain a qualitative indicator of condensation patterns. However, a more realistic assessment of these relative humidity contours must be made by comparing with the specific airplane geometry for which condensation data are available, as well as by incorporating condensation effects into the modeling equations.

Airplane Flow Patterns

Some additional examples of the inflight photographs are presented to illustrate the variety of airplane flow patterns that have been visualized by the condensation process. The complete collection of photographs obtained for this study show patterns for a large number of airplanes through a range of flight conditions. However, because of the large number of photographs involved, only a few have been selected for presentation herein.

High Speed Flows

Transonic flows around fighter aircraft occur for a wide range of speed and maneuver conditions. Two examples are presented in Fig. 7, which shows an F-18 in a high speed pull up and an F-4 in a high speed pass over a runway. The condensed patterns are similar to the patterns obtained for the F-14 (Fig. 5a), where the flow condenses in the expansion region and evaporates as the flow goes through the shock wave. The resulting pattern is often referred to as a Mach diamond.

Comparing the condensed flow patterns for the F-18 and F-4 leads to several observations. At low angles of attack and high subsonic speed, the F-4 has supercritical flow above and

below the airplane and the shock wave appears to be essentially perpendicular to the fuselage. Unlike the F-4, the F-18 has condensation only over the upper part of the airplane, which is due to having much less expansion on the lower surface. In addition, the shock wave for the F-18 slopes forward, which is indicative of a lower subsonic Mach number than the F-4. Both aircraft have condensation occurring over their canopies, because of the flow expansion in that area.

Condensation patterns, even vortex flows, can occur at supersonic speeds, as evidenced by the photograph of the B-70 bomber presented in Fig. 8. As can be seen, condensed vortex flows originate from the canard, and the outer wing panel dihedral break of a B-70 at supersonic speeds, which is deflected down about 25 deg. The canard vortices appear to thin out as they pass over the aft end of the vehicle, which is probably due to its passing through the trailing shock wave. Additionally, there is condensation over the forward fuselage and canard due to flow expansions. The trailing-edge flaps are deflected down together with an up deflection of the canard for longitudinal control.[45] The expansion over the trailing-edge flaps also results in flow condensation.

Vortical Flows

Wing-Body Strake and Glove

Wing-body strakes and gloves are slender, highly-swept airplane surfaces that can develop lead-edge vortices. At the intersection of the wing-body strake, or glove, with the wing, the virtical flow sheds downstream and passes over the aft wing and tail surfaces. Examples of this class of condensed vortex flow are illustrated for wing-body strake vortices on the F-16 fighter at maneuver conditions Fig. 9a, and for the glove vortices on the B-1 bomber at a high lift condition in Fig. 9b. The wing-body strake on the F-16 fighter is a thin, aerodynamically-sharp surface designed to generate a strong vortex to enhance maneuver performance. On the other hand, the glove on the B-1 bomber has a thick, rounded leading-edge, which is designed to delay leading-edge separation. The B-1 glove has a leading-edge sweep angle of about 70 deg so that the flow separates at a moderate angle of attack to yield the glove vortices noted in the figure.

Multiple Interacting

Variable sweep and double-delta type of wing planforms can have vortices generated by inboard and outboard planforms with different sweep angles. These vortices interact with each other as they flow over the wing. The flows about the F-14 (Fig. 10a) and the SR-71 (Fig. 10b) are good examples of multiple vortex interactions. On the F-14, vortices are generated inboard on the glove and glove-vane, which is extended for this case of high wing sweep, and outboard on the wing panel.

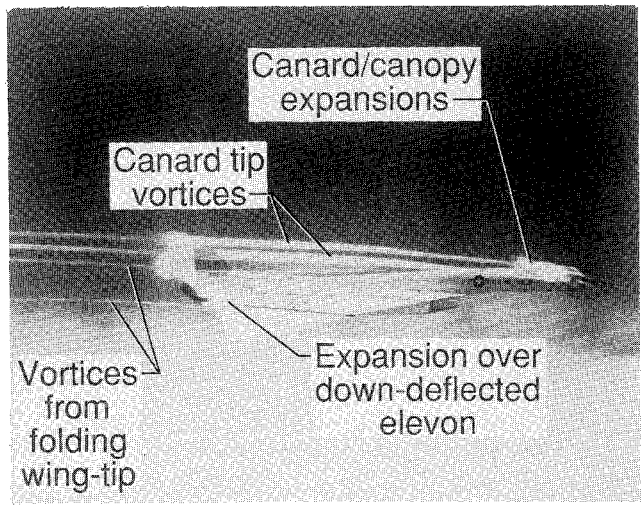

Fig. 8 Condensation patterns on the B-70 bomber airplane at supersonic cruise.

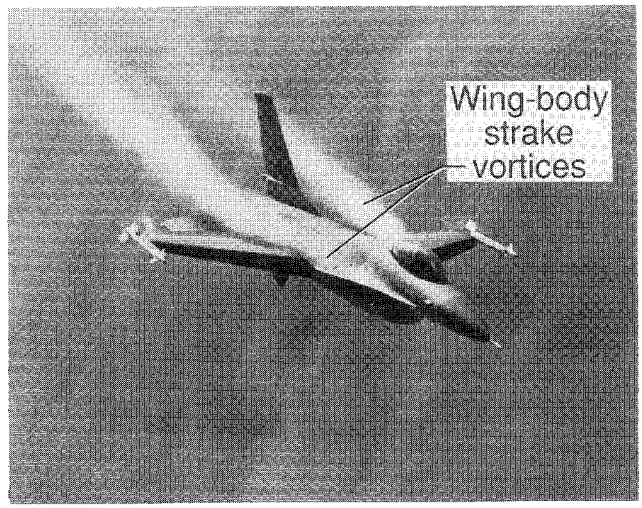

a) Wing-body strake vortices on F-16 during maneuver

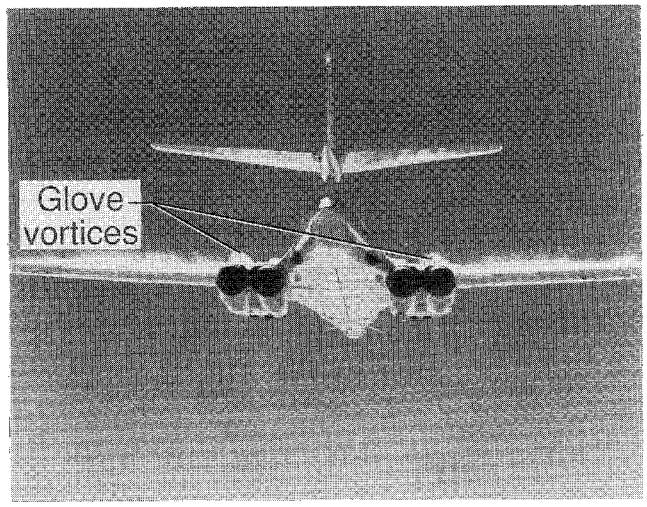

b) Glove vortices on B-1 with wings at unswept position

Fig. 9 Condensed vortex flows generated by wing-body strakes on a fighter and by gloves on a bomber.

On the SR-71, leading-edge vortex flows are generated from the chine on the engine nacelle and from the outboard wing panel. Since the two vortices are corotating, i.e., rotate in the same direction, the vortex flows rotate about each other. The outer-panel vortex is displaced upward and inboard, while the chine vortex is displaced downward and outboard to form the spiraling pattern in the photograph.

Streamwise Vorticity from Wing Leading-Edges

Condensation can occur in streamwise vorticity that is shed from wing leading-edges of transport and fighter airplanes as is shown in Fig. 11. The small streamwise vortices were observed on the inboard portion of wing of the Boeing 737 transport (Fig. 11a) during climb-out with its wing leading-edge devices retracted. It is believed that this pattern is initiated in the wing leading-edge region and is related to the growth of the three-dimensional, boundary-layer, cross-flow instability vortices, which are corotating and streamwise. Poll[46] has recently studied these vortices for their implications on the three-dimensional boundary-layer transition process.

A similar condensation pattern was obtained for the F-18 (Fig. 11b), where the wing leading-edge and trailing-edge flaps are deflected for a maneuver condition. The vorticity is shed streamwise from the leading-edge region and spanwise over the whole wing, although the size and spacing appears to be

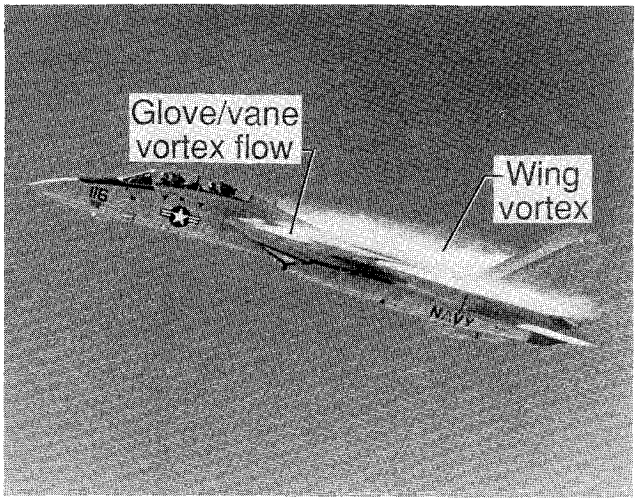

a) F-14 during maneuver with wings swept aft

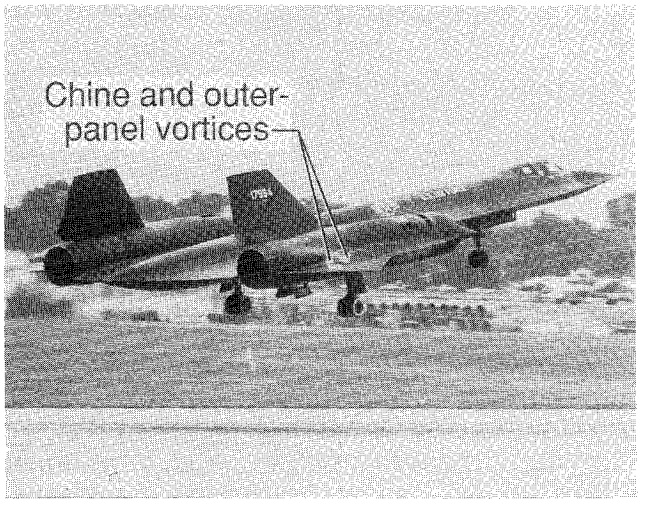

b) SR-71 at landing

Fig. 10 Multiple interacting leading-edge vortex flows on fighter and supersonic-cruise aircraft F-14 during maneuver with wings swept aft

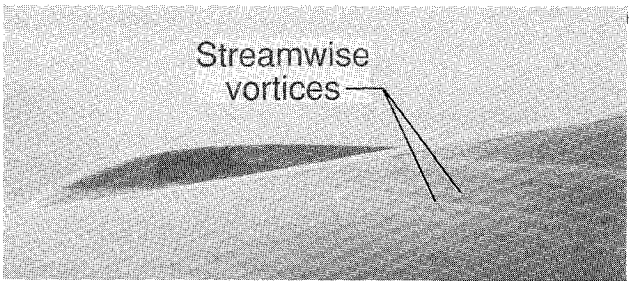

a) Boeing 737 transport during climbout

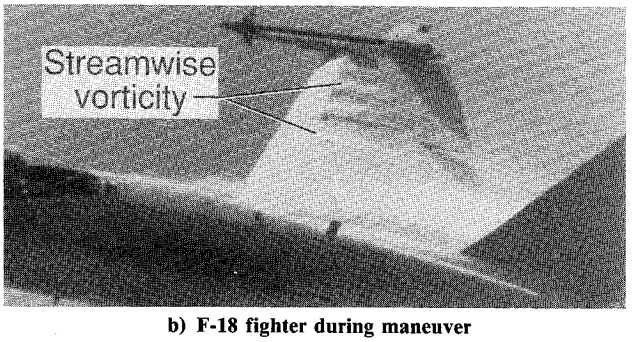

b) F-18 fighter during maneuver

Fig. 11 Streamwise vorticity from wing leading-edges of transport and fighter airplanes.

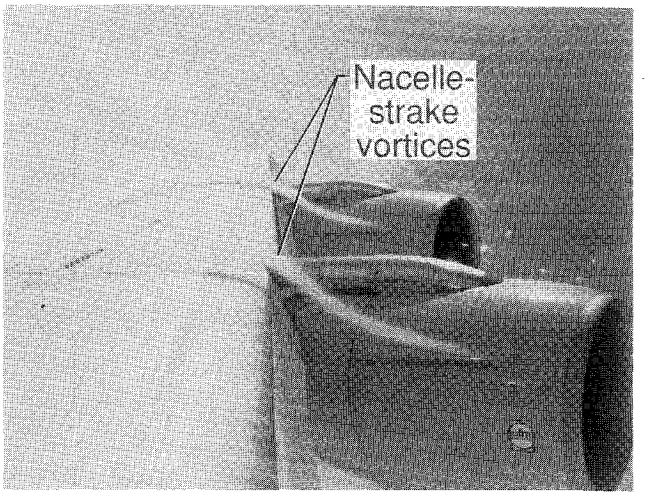

a) Favorable: Boeing 707 nacelle strakes at high lift

b) Unfavorable: propulsion-induced ground vortices on YC-14

Fig. 12 Favorable and unfavorable vortex flows generated by transport airplanes.

larger than observed on the transport. For both aircraft, the condensation pattern appears to stop at the wing midchord. This effect is interpreted to be the result of the upper surface flow compressing as it approaches the trailing-edge, which could increase temperature and cause evaporation. The streamwise vortices themselves would be expected to continue over the wing and into the wing wake.

Vortex Generation

The condensation patterns shown in Fig. 12 illustrate several ways that vortex flows are generated in manners that can help or hinder the performance of transport airplanes. In Fig. 12a, small strakes were located on the inboard side of the nacelles of a Boeing 707 to generate strong vortices that pass over the wing upper surface to improve wing flow at the high-lift conditions with the leading-edge devices deflected down. The strake vortices help control separated flow off of the nacelles at high lift, which reduces the airplane's approach speed and landing field lengths.[47]

Note that the vortex cores are clear of condensed flow, and appear like hollow tubes. A possible explanation for this was discussed previously for the leading-edge vortex calculations for a delta wing. The analysis showed that the core relative humidity was less than 1, which leads to vaporization. Another influence is due to centrifugal effects which move condensed particlesl out of the core. Mueller[11] describes this process for smoke particles.

An engine can induce a ground, or starting vortex, if the propulsion unit has enough power and/or is close enough to the ground. This undesirable type of vortex flow is dramatically illustrated by the YC-14 (Fig. 12b), where ground vortices are being induced into the propulsion inlets, especially on the right side. This flow environment around the inlet creates problems of ingesting foreign objects[48,49] and is a safety hazard for ground personnel working near transports and fighters. Fighters are very susceptible to this problem since their jet engines are in close proximity to the runway or carrier deck.

Vortices from Edges

Vortices that are generated at wing tips and at the side edges of trailing-edge flaps are among the most commonly observed condensed flow patterns. The examples shown in Figs. 13a and 13b are for a Jaguar aircraft during a maneuver, and a DC-9 during landing, respectively. These vortices are typically observed at take off, landings, and maneuver at low altitude where they can be seen by ground observers. There is a regular pattern that occurs in the tip vortices of the Jaguar, which is not currently understood.

Engine Inlet Related

At some maneuver conditions, fighter airplanes can generate vortex flows that originate near their engine inlets that may affect inlet performance as well as interact with aft surfaces. The flow expands through the F-4 boundary-layer diverters and condenses to create the vortex flow pattern shown in Fig. 14a. In addition, a vortex appears to be generated from the F-14 inlet cowl (Fig. 14b), which then passes over the glove and horizontal tail surfaces. The inlet cowl vortex was observed in a water tunnel test of an F-14 model.[50] The condensation patterns suggest that an additional vortex is created at the missile launch rail located on the underside of the glove.

Correlation with Tunnels

Several comparisons of flight and tunnel flow patterns are shown to demonstrate similarities and differences between the full scale flight condensed flow patterns and the smaller scale tunnel results. Existing techniques, such as smoke in wind tunnels and dyes in water tunnels, have been used for a number of years and have matured to an acceptance level by the research community.

LEX Vortex Flow

Vortex burst is a common aerodynamic phenomenon that occurs at some angles of attack for all leading-edge vortex flows. An F-18 leading-edge extension (LEX) has a strong vortex flow that bursts upstream of the vertical tails at high angles of attack. The flow patterns are illustrated in Fig. 15a for the airplane in flight, and in Fig. 15b for a scale model in a water tunnel. The flight condensation pattern shows the LEX vortex that appears to end in mid air. Of course, the vortical flow continues on beyond the burst point, which is illustrated by dyes in an experiment by Erickson[51] in the Northrop water tunnel with $\alpha = 32$ deg.

The reason for the disppearance of the condensed flow near the vortex burst point is probably due to the fact that there is an adverse pressure gradient and deceleration of flow,[43,52]

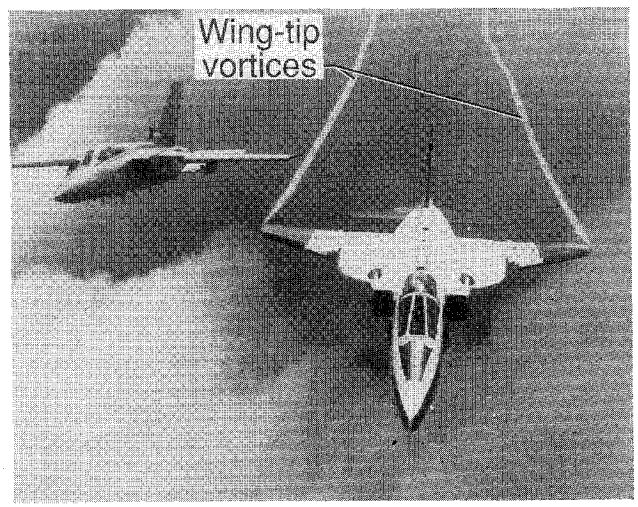

a) Wing-tip vortices on Jaguar during maneuver

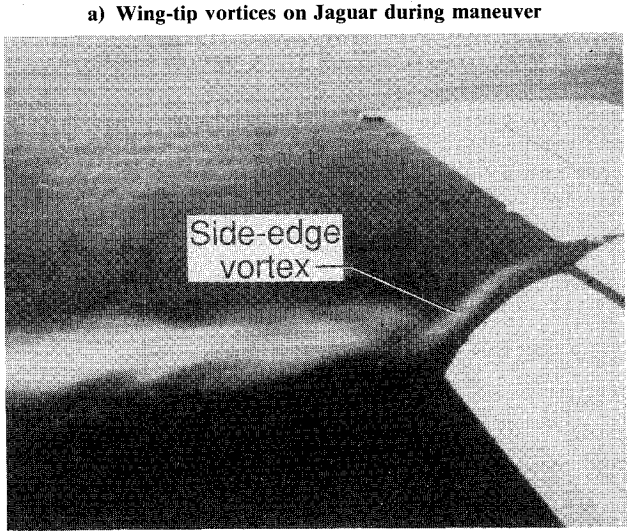

b) Vortex from side edge of trailing-edge flap of DC-9 during landing

Fig. 13 Vortex flows from the edges of wings and flaps for transport and fighter airplanes.

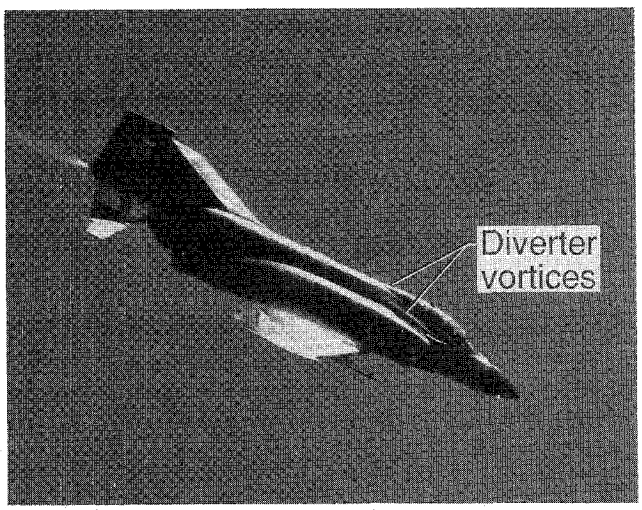

a) F-4 boundary-layer diverter vortices

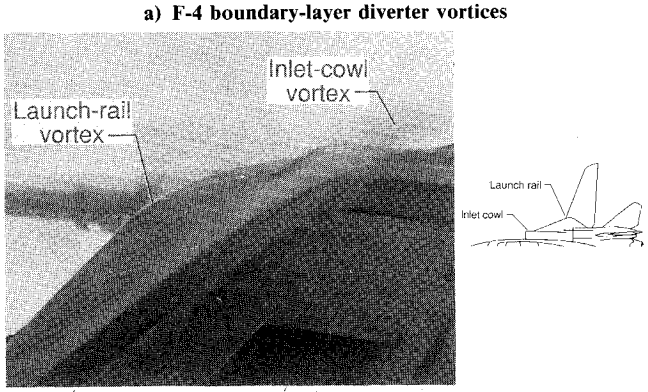

b) F-14 engine inlet-cowl vortex

Fig. 14 Vortex flows generated near engine inlets for several fighter airplanes during maneuver.

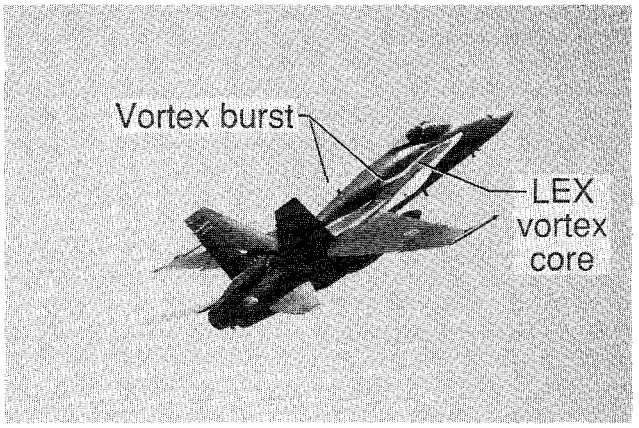

a) Flight condensation during maneuver

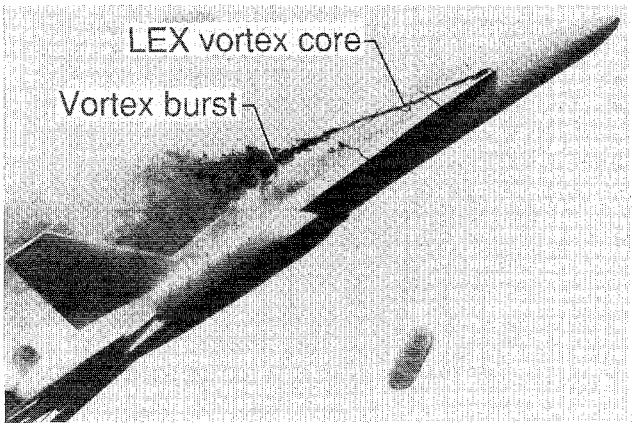

b) Water tunnel dyes, $\alpha = 32$ deg

Fig. 15. Vortex burst on an F-18 configuration visualized with condensation in flight and dyes in a water tunnel.

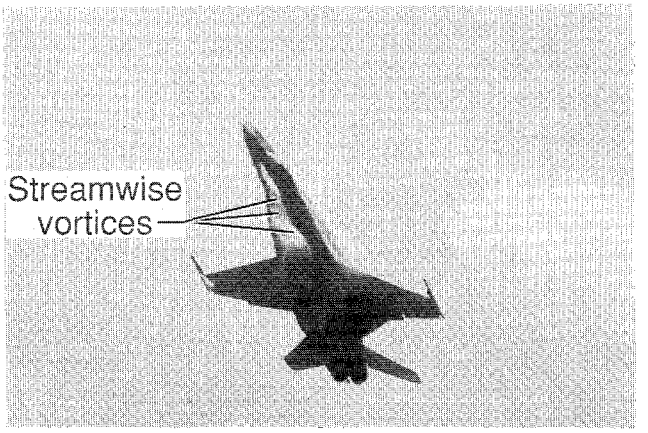

a) LEX vortex flow on F-18, flight condensation during maneuver

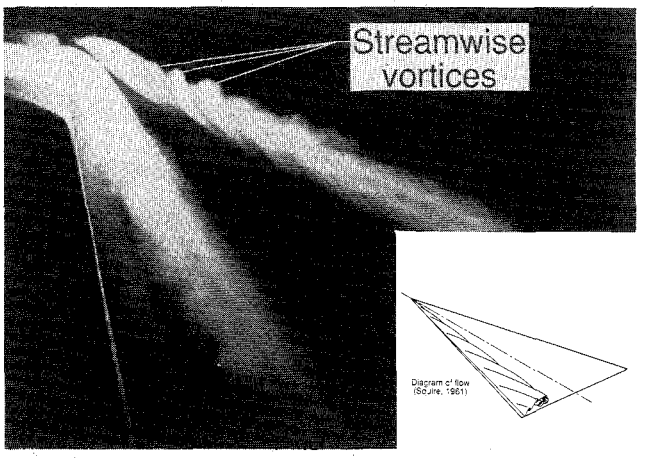

b) Leading-edge vortex flow on 75 deg delta wing, wind tunnel smoke, $\alpha = 20$ deg

Fig. 16 Streamwise vortices in separated shear layer visualized with flight condensaton and with wind tunnel smoke.

which causes a rise in pressure and temperature that is great enough to cause evaporation to occur. A similar process occurs for condensed flow that vaporizes at a shock wave, as discussed previously. This suggests that caution should be exercised when comparing flows visualized by condensation with those by seeding, like dyes or smoke.

Streamwise Vortices in a Separated Shear Layer

When the flow separates from a slender, highly-swept leading-edge, a shear layer, or vortex sheet, is formed. This shear layer is often depicted as a sheet with no substructure or detail apparent. However, in recent low-speed wind tunnel research, Payne[52] used smoke to visualize streamwise vortices in the leading-edge vortex sheet, as shown in Fig. 16b for a 75 deg delta wing at $\alpha = 20$ deg. These secondary vertical structures follow a helical path in the shear layer as suggested by the sketch of Squire et al.[53] Comparable secondary vortical structures are shown in Fig. 16a for the condensed LEX vortex flow on an F-18.

This is the first occasion for this photographic evidence to be made available to the research community, and suggests that the vortex structure that had been researched at lower Reynolds number in a wind tunnel (8.5×10^4) does occur in flight at full-scale Reynolds number. Thus the in-flight condensation patterns can be useful for research information even when the flight conditions for the photographs are unknown.

Future Research

Additional studies are required to help validate in-flight condensation as an acceptable flight flow visualization technique. First of all, accurate flight and atmospheric conditions are needed to make the photographic information more usable for steady and unsteady maneuvers.

Flight and wind tunnel experiments are needed to determine what conditions are necessary for condensation to occur as a function of flight envelope, i.e., speed and altitude, atmospheric conditions, and airplane geometries. This may require some new wind tunnel and flight test techniques to be developed to answer some of these questions, although portions of existing flow visualization techniques should be adaptable to studying condensation. This information would also help evaluate the usefulness of the simple relative humidity formulation that is used in this paper.

Detailed research could help determine what effect condensing and evaporating flow has on the flowfield. That is, does the presence of condensation alter the thermodynamics enough to change the pressure distribution over the aircraft? Answering this question would also determine if a more accurate formulation of the condensation process is necessary.

Additional comparisons should be made between condensation patterns and other forms of flow visualization in flight and tunnels to investigate the strengths and weaknesses between the techniques for a variety of flowfields.

Conclusions

Flight condensation patterns illustrate a variety of airplane flowfields, such as attached and separated flows, vortex flows, and expansion and shock waves. These patterns are a unique source of flow visualization that has not been generally utilized previously.

Calculating relative humidity by post-processing solution fields obtained with standard computational codes provides a qualitative indicator of the condensation pattern.

Analysis shows vortex cores have a low relative humidity (<1), which may help explain the voids in condensed vortex flows.

The analysis also revealed that relative humidity is more sensitive to changes in local static temperature than to changes in pressure.

The relative humidity formulation must be compared with specific wind tunnel and/or flight geometries where condensation data are available. A more complete theoretical modeling may be necessary to obtain details of the condensation process.

Flight condensation patterns at full-scale Reynolds number can provide useful information for researchers experimenting in sub-scale tunnels.

Some observations of the in-flight condensed flow patterns are: 1) vortex burst can evaporate the condensed LEX vortex flow; and 2) streamwise vortices were observed in separated shear layers on a LEX vortex.

Acknowledgments

Flight condensation photographs were provided by the following photographers, individuals, and organizations:

- Aviation Week and Space Technology; F-16, Fig. 1a
- NASA Dryden; TACT, Fig. 4a
  E. W. Schoonover, NASA Langley; flight condition
- Paul A. Ludwing; F-14, Fig. 5a
- Air France; Concorde, Fig. 6a
- Frank B. Mormillo; F/A-18, Fig. 7a
  Harry Gann, McDonnell-Douglas; F-4, Fig. 7b
- NASA Dryden; B-70, Fig. 8
- General Dynamics; F-16, Fig. 9a
  A. Schoenheit, Rockwell; B-1B, Fig. 9b
- Frank Mormillo; F-14, Fig. 10a
  Chuck Mayer; SR-71, Fig. 10b
- Stephen Wolf; 737, Fig. 11a
  McDonnell Douglas Corp.; F-18, Fig. 11b
- H. Yoshihara, Boeing; 707, Fig. 12a
  USAF, via Charles Boppe, Grumman; YC-14, Fig. 12b
- British Aerospace; Jaguar, Fig. 13a
  J. A. Blackwell, Lockheed; DC-9, Fig. 13b
- Steven Wolf; F-4, Fig. 14a
  Steven Zini; F-14, Fig. 14b
- K. Tokunaga, Japan; F-18, Fig. 15a
- Eddy Mets; F-18, Fig. 16a

References

[1]Maltby, R. L., "Flow Visualization in Wind Tunnels Using Indicators," *AGARDograph* 70, April 1962.

[2]McGregor, I., "The Vapor-Screen Method of Flow Visualization," *Journal of Fluid Mechanics,* Vol. 11, Pt. 4, Dec. 1961, pp. 481–511.

[3]Sedney, R., Kitchens, C. W., and Bush, C. C., "Combined Techniques for Flow Visualization," AIAA Paper 76-55, Jan. 1976.

[4]Settles, G. S., "Flow Visualization Techniques for Practical Aerodynamic Testing," *Flow Visualization III,* edited by W. J. Yang, *Proceedings of the Third International Symposium on Flow Visualization,* Hemisphere, New York, pp. 306–315.

[5]Nelson, R. C., "Flow Visualization of High Angle of Attack Vortex Wake Structures," AIAA Paper 85-0102, Jan. 1985.

[6]Hunter, W. W. and Foughner, J. T. (eds), "Flow Visualization and Laser Velocimetry for Wind Tunnels," NASA CP-2243, March 1982.

[7]Record of the International Congress on Instrumentation in Aerospace Simulation Facilities (ICIASF), Williamsburg, VA, June 1987.

[8]Van Dyke, M., *An Album of Fluid Motion,* Parabolic Press, Stanford, CA, 1982.

[9]Crowder, J. P., "Wake Imaging System Applications at the Boeing Aerodynamics Laboratory," Society of Automotive Engineers Paper 851895, Oct. 1985.

[10]Miller, D. S. and Wood, R. M., "Lee-Side Flow Over Delta Wings at Supersonic Speeds," NASA TP-2430, June 1985.

[11]Mueller, T. J., "Smoke Visualization of Subsonic and Supersonic Flows," University of Notre Dame, Notre Dame, IN, UNDAS TN-3412-1, June 1978.

[12]Payne, F. M., Ng, T. T., Nelson, R. C., and Schiff, L. B., "Visualization and Wake Surveys of Vortical Flow Over a Delta Wing," *AIAA Journal,* Vol. 26, Feb. 1988, pp. 137–143.

[13]Wentz, W. H., Jr. and Kohlman, D. L., "Wind-Tunnel Investigation of Vortex Breakdown on Slender Sharp-Edged Wings," NASA CR-98737, Nov. 1968.

[14]Kjelgaard, S. O., Sellers, W. L., and Weston, R., "The Flowfield Over a 75 Degree Swept Delta Wing at 20.5 Degrees Angle of Attack," *Proceedings of the AIAA 4th Applied Aerodynamics Conference,* AIAA, New York, June 1987.

[15]Chambers, J. R., "High-Angle-of-Attack Aerodynamics: Lessons Learned," AIAA Paper 86-1775, June 1986.

[16]Hughes, J. P., Brumby, R. E., and Belevtsov, N., "Flow Visualization from the Ground Up," AIAA Paper 83-2691, Nov. 1983.

[17]Fenell, L. J., "Vortex Breakdown—Some Observations in Flight on the HP 115 Aircraft," R&M No. 3805, British Aeronautical Research Council, 1977.

[18]Crowder, J. P., "Flow Visualization Techniques Applied to Full Scale Vehicles," presented at the Fourth International Symposium on Flow Visualization, Paris, France, Aug. 1986.

[19]Lamar, J. E., et al., "In-Flight Flow Visualization of F-106B Leading-Edge Vortex Using the Vapor Screen Technique," AIAA Paper 86-0785, April 1986.

[20]Burdin , I., et al., "Use of Laser Methods for the Study of Separated Flow in the Wind Tunnel and in Flight," (Foreign Technology Division, Wright-Patterson Air Force Base, translated) FTD-ID(RS) T-1053-82, U.S. Air Force, Oct. 1982. (Available from DTIC as AD B069 459).

[21]Asanuma, T., *Proceedings of the International Symposium on Flow Visualization,* Hemisphere, New York, 1977.

[22]Merzkirch, W. (ed.), *Proceedings of the Second International Symposium on Flow Visualization,* Bochum, West Germany, Sept. 1980.

[23]Yang, W. J. (ed.), "Flow Visualization III," *Proceedings of the Third International Symposium on Flow Visualization,* Hemisphere, New York, 1983.

[24]Veret, C. (ed.), "Flow Visualization IV," *Proceedings of the Fourth International Symposium on Flow Visualization,* Hemisphere, New York, 1986.

[25]AIAA 3rd Flight Testing Conference and Technical Display, Las Vegas, NV, April 1986.

[26]17th Annual Symposium, Society of Flight Test Engineers, Society of Experimental Test Pilots, Lancaster, CA.

[27]30th Symposium, Experimental Test Pilots, Society of Experimental Test Pilots, Lancaster, CA.

[28]Wegener, P. P. and Mack, L. M., "Condensation in Supersonic and Hypersonic Wind Tunnels," *Advances in Applied Mechanics,* Vol. V, 1958, pp. 307–445.

[29]Pope, A. and Goin, K. L., *High Speed Wind-Tunnel Testing,* Wiley, New York, 1965.

[30]Wegener, P. P., "Gasdynamics of Expansion Flows with Condensation and Homogeneous Nucleation of Water Vapour," *Nonequilibrium Flows,* Ch. 4, Pt. 1, Marcel Dekker, New York, 1970, pp. 163–243.

[31]Reed, T. D., Pope, T. C., and Cooksey, J. M., "Calibration of Transonic and Supersonic Wind Tunnels," NASA CR-2920, Nov. 1977.

[32]Jordan, F. L., "Investigation at Near-Sonic Speed of Some Effects of Humidity on the Longitudinal Aerodynamic Characteristics of an NASA Supercritical Wing Research Airplane Model," NASA TMX-2618, 1972.

[33]Jordan, F. L., "Investigation of Some Effects of Humidity on Aerodynamic Characteristics of a 10-Percent-Thick NASA Supercritical Airfoil," NASA TMX-3355, 1976.

[34]Hall, R. M., "Real Gas Effects II—Influence of Condensation on Minimum Operating Temperatures of Cryogenic Wind Tunnels," *Cryogenic Wind Tunnels,* AGARD LS No. 111, 1980.

[35]Hall, R. M., "Studies of Condensation Effects on Airfoil Testing in the Langley 0.3-Meter Cryogenic Tunnel," NASA TP-2509, Jan. 1986.

[36]Robinson, C. E., Bauer, R. C., and Nichols, R. H., "Estimating Water Vapor Condensation Effects for Transonic and Supersonic Flow Fields," AIAA Paper 85-5020, Oct. 1985.

[37]Van Wylen, G. J., *Thermodynamics,* Wiley, New York, April 1960, Chap. 9, pp. 203–209.

[38]Rumsey, C. L., Taylor, S. L., and Thomas, J. L., "Application of an Upwind Navier-Stokes Code to Two-Dimensional Transonic Airfoil Flow," AIAA Paper 87-0413, 1987.

[39]Symposium on Transonic Aircraft Technology (TACT), Air Force Flight Dynamics Lab., TR-78-100, Wright-Patterson AFB, Aug. 1978.

[40]Anderson, W. K., Thomas, J. L., and Rumsey, C. L., "Extension and Applications of Flux-Vector Splitting to Unsteady Calculations on Dynamic Meshes," AIAA Paper 87-1152, June 1987.

[41]Thomas J. L. and Anderson, W. K., "Implicit Characteristic-Based Scheme for Large-Scale Computations," Euler Solvers Workshop, Monterey, CA, Aug. 1987.

[42]"Condensation of Water Vapor Makes F-14 Shock-Waves Visible," *Aviation Week and Space Technology,* Nov. 1977, pp. 46-47.

[43]Thomas, J. L., Taylor, S. L., and Anderson, W. K., "Navier-Stokes Computations of Vortical Flow Over Low Aspect Ratio Wings," AIAA Paper 87-0207, 1987.

[44]Hummel, D., "On the Vortex Formation Over a Slender Wing at Large Angles of Incidence," AGARD CP-247, Paper 15, Feb. 1983.

[45]Peterson, J. B. et al., "Wind-Tunnel/Flight Correlation Study of Aerodynamic Characteristics of a Large Flexible Supersonic Cruise Airplane (XB-70-1); II—Extrapolation of Wind-Tunnel Data to Full-Scale Conditions," NASA TP-1515, Feb. 1980.

[46]Poll, D. I. A., "Transition Description and Prediction in Three-Dimensional Flows," Paper 5, special course on Stability and Transition of Laminar Flow, AGARD-R-709, March 1984.

[47]Stein, D. E., "Vortex Generators: Case History—Use of Vortex Generators in Aircraft Design," *Airliner,* Oct.-Dec. 1985.

[48]Bulluck, D., "The Volatile Vortex," *Flying Safety,* Sept. 1986, p. 11.

[49]Glenny, D. E. and Pyestock, N. G. T. E., "Ingestion of Debris into Intakes by Vortex Action," Aeronautical Research Council, CP 1114.

[50]Lorincz, D. J., "Flow Visualization Study of the F-14 Fighter Aircraft Configuration," NASA CR-163098, Sept. 1980.

[51]Erickson, G. E., "Water Tunnel Flow Visualization and Wind Tunnel Data Analysis of the F/A-18," NASA CR-165859, May 1982.

[52]Payne, F. M., "The Structure of Leading Edge Vortex Flows Including Vortex Breakdown," Ph.D. Dissertation, Dept. of Aerospace and Mechanical Engineering, University of Notre Dame, Notre Dame, IN, May 1987.

[53]Squire, L. C., Jones, J. G., and Stanbrook, A., "An Experimental Investigation of the Characteristics of Some Plane and Cambered 65° Delta Wings at Mach Numbers from 0.7 to 2.0," R&M 3305, British ARC, 1963.

Color reproduction courtesy of NASA Langley Research Center.